



CHORUS

This is the accepted manuscript made available via CHORUS. The article has been published as:

Chemically and electrically tunable spin polarization in ferroelectric Cd-based hybrid organic-inorganic perovskites

Ravi Kashikar, P. S. Ghosh, S. Lisenkov, B. R. K. Nanda, and I. Ponomareva

Phys. Rev. B **104**, 235132 — Published 17 December 2021

DOI: [10.1103/PhysRevB.104.235132](https://doi.org/10.1103/PhysRevB.104.235132)

Chemically and electrically tunable spin-polarizations in ferroelectric Cd-based hybrid organic-inorganic perovskites

Ravi Kashikar,^{*} S. Lisenkov, and I. Ponomareva[†]

Department of Physics, University of South Florida, Tampa, Florida 33620, USA

P. S. Ghosh

*Department of Physics, University of South Florida, Tampa, Florida 33620, USA and
Glass & Advanced Materials Division, Bhabha Atomic Research Centre, Mumbai 400 085, India*

B. R. K. Nanda

*Condensed Matter Theory and Computational Lab, Department of Physics,
Indian Institute of Technology Madras, Chennai 600036, India and
Center for Atomistic Modelling and Materials Design,
Indian Institute of Technology Madras, Chennai 600036, India*

(Dated: December 3, 2021)

Density functional theory computations are used to predict electronic structure of Cd-based hybrid organic-inorganic high T_C ferroelectric perovskites with TMCM-CdCl₃ being one representative. We report Rashba-Dresselhaus spin-splitting in the valence band of these nonmagnetic compounds. Interestingly, we find in computations that the splitting is not necessarily sensitive to the polarization of the material but to the organic molecule itself which opens a way to its chemical tunability through the choice of the molecule. Further chemical tunability of spin-splitting is shown to be possible through substitution of Cl in the CdCl₃ chains as the valence band was found to originate from Cl-Cl weakly bonding orbitals. For example, substitution of Cl with Br in TMCM-CdCl₃ resulted in ten times increase of spin-splitting. Furthermore, the spin-polarization in these materials give origin to persistent spin textures which are coupled to the polarization direction, and, therefore can be controlled by the electric field. This is promising for spintronics applications.

I. INTRODUCTION

Ferroelectrics are the materials that exhibit spontaneous polarization in the absence of the electric field. They find numerous applications in dynamic random access memories, transduction sensors and actuators [1, 2]. Recently, cofunctionality between ferroelectricity and Rashba spin-splitting has been established in GeTe [3–6] and predicted in several ferroelectrics [7–13]. Such cofunctionality is understood as the coexistence of ferroelectricity and spin-polarization in the same material and typically implies the possibility to control the latter by the direction and/or magnitude of ferroelectric polarization. For example, reversal of polarization by the electric field has been shown to result in the reversal of the spin-texture direction [7, 14]. Such co-functionality is very attractive for nonvolatile spintronic devices [14]. However, so far it has been explored mostly in inorganic ferroelectrics.

Hybrid organic inorganic ferroelectrics/piezoelectrics are recently emerging as an attractive alternative to the traditional inorganic ones as they feature several advantages: lack of toxic elements, flexibility, low synthesis temperature, and larger chemical tunability [15–18]. Can these materials also exhibit the aforementioned spin-polarization/ferroelectricity co-functionality? Very

limited insights are available at the moment. Switchable Rashba bands have been predicted for the basic halide perovskite ferroelectrics family [19]. More recently, Lou *et al.* [20] used density functional theory (DFT) calculations to predict Rashba-like band splitting and persistent spin textures in antiferromagnetic hybrid organic inorganic perovskite (HOIP) TMCM-MnCl₃ (TMCM=trimethylchloromethyl ammonium). Remarkably, the spin textures were found to be tunable by switching the magnetic ordering or ferroelectric polarization. The family of TMCM-MnCl₃, TMCM-CdCl₃ and TMC_{1-x}F_xM-CdCl₃ materials is very attractive as they exhibit high Curie temperature, large piezoelectric response [15, 17], which was predicted to originate from phase switching [21], and property tunability by pressure [22]. This impressive diversity of co-functionalities suggests further investigation into the possibility to observe electrically tunable spin-polarizations and spin-textures in its non-magnetic members, TMCM-CdCl₃ and TMC_{1-x}F_xM-CdCl₃ which, to the best of our knowledge, has not been reported this far. Furthermore, it is presently unknown whether the spin-polarizations in cofunctional hybrid ferroelectrics are chemically tunable. Motivated to fill up this gap in understanding of non-magnetic Cd-based HOIP we aim: (i) to predict that they exhibit band-splitting, spin polarizations and electrically tunable spin textures; (ii) to predict chemical tunability of these properties and its atomistic origin; (iii) to reveal the nontrivial role that the organic molecule plays in the effect. The rest of the paper is organized as fol-

^{*} ravik@usf.edu

[†] iponomar@usf.edu

lows: in Section II, we present computational details; in Section III, we focus on changes in the band structure of perovskite due to large structural distortions associated with the formation of HOIP structure; in Section IV, we present spin-splitting and spin-polarization in Cd-based HOIP; and in Section V, we predict their chemical and electrical tunability. In Section VI, we summarize the work.

II. COMPUTATIONAL DETAILS

DFT based pseudopotential methodology with Perdew-Burke-Ernzerhof (PBE) exchange-correlation functional [23] as implemented in Vienna Ab-initio Simulation Package (VASP) [24] was utilized for this study. The electron-ion interactions are treated with the projected augmented wave (PAW) potentials [25]. Zero damping D3 dispersion corrections as proposed by Grimme *et al.* [26] are incorporated in the simulations. A cutoff energy of 700 eV for the plane wave basis set is used and a $4 \times 2 \times 4$ Monkhorst-Pack k-point mesh is employed for the integration over the Brillouin zone. This choice ensures energy convergence of 0.002 eV/f.u. All structural relaxations are carried out using conjugate gradient algorithm until ionic forces are less than 2 meV/Å, which results in residual stresses less than 0.05 GPa. All the electronic structure calculations are carried out with spin-orbit coupling (SOC), unless specified. The polarization is computed using modern theory of polarization developed by King-Smith and Vanderbilt [27].

III. BAND STRUCTURE OF HIGHLY DISTORTED PEROVSKITE

Let us begin by inspection of TMCM-CdCl₃ structure given in Fig. 2(a) and notice that it is rather different from the prototypical perovskite ABX₃. Therefore, it is imperative to understand what structural transformations relate this structure to prototypical perovskite ABX₃ and what effect they may have on its electronic structure. To address this question we look into two inorganic counterparts of TMCM-CdCl₃: cubic CsCdCl₃ (shown in Fig. 1(a)) and a hypothetical monoclinic CsCdCl₃ (see Fig. 1(b)) that has the same space group as the TMCM-CdCl₃ ground state. The fully relaxed cubic CsCdCl₃ has the lattice parameter 5.32 Å, which agrees well with the experimental value 5.22 Å [28, 29]. The crystal structure and the orbital resolved band structure of cubic CsCdCl₃ are shown in Figure 1. The following observations can be made from the band structure: (i) The band structure around the Fermi level (E_F) is dominated by Cd- $\{s, p\}$ and Cl- p valence orbitals, which undergo covalent hybridization to create highly dispersive antibonding and bonding bands lying higher and lower in energy respectively with a set of weakly dispersive bands

in the middle [30]. With 18 valence electrons per unit cell, the E_F lies between Cl- p dominated weakly bonding and Cd- s dominated antibonding states. The conduction band minimum and valence band maximum are formed at Γ and R respectively to create an indirect bandgap of 1.7 eV. The cubic to monoclinic structural transformation can be understood from the projection of the cubic perovskites along the [111] direction as shown in Fig. 1(a). The alternate stacking of Cs and Cd layers gives rise to a triangular-hexagonal pattern. In the monoclinic phase, as shown in Fig. 1(b), the redistribution of Cs and Cd occurs where the columns of Cd lying at the center of each hexagon formed by the Cs atoms. Such a transformation distorts the octahedra significantly and isolate them in the ab -plane, while a chain of them is formed along the c -axis. The lack of axial Cd-Cl-Cd covalent bonding involving the p -orbitals, both due to isolation and distortion, resulted in the formation of narrow bands as reflected in Fig. 1(d) and (e). We estimated the band width of a valence band in the monoclinic phase to be in the range 0 - 0.2 eV, whereas in the cubic phase it can be as large as 3 eV.

IV. SPIN-SPLITTING AND SPIN-POLARIZATIONS IN CD-BASED HOIP

Having achieved the basic understanding of the role structural distortion play in the electronic structure of the inorganic counterparts we turn to TMCM-CdCl₃. The calculations were carried out on the fully relaxed TMCM-CdCl₃ structure (Cc space group), whose parameters are the ones previously reported by us in Ref.21 and agree well with experimental values at 293 K [17]. They are 9.3 Å, 15.5 Å, 6.9 Å and $\beta = 94.6^\circ$. We direct x -, y -, and z -axis along a , b and c crystallographic directions, respectively. The structure is shown in Fig. 2a, whose local environment and orbital interactions resemblance to the inorganic CsCdCl₃. The orbital resolved band structure computed without incorporation of SOC is presented in Fig. 2b. The lowest conduction band is of Cd- s ($\sim 65\%$) and Cl- p ($\sim 35\%$) orbital characters with minimum at the Γ point. This is in contrast with Cd- s dominated orbital character of cubic CsCdCl₃ conduction band and is attributed to the distortion of the octahedral cage. The valence band spectrum is of predominantly Cl- p orbital character and small fraction of Cd- d orbital character with maximum at Γ point. The valence band spectrum is less dispersive as compared to conduction band spectrum due to the weakly bonded nature of Cl- p orbitals. The calculations predict a direct band gap of 4.35 eV which could be compared with experimental value of 5.51 eV [31]. The band gap is enhanced with respect to cubic CsCdCl₃ due to the aforementioned octahedral isolations and large scale distortions that decrease the orbital overlap strength. It should be noted that further improvement in the band gap prediction can be achieved by using hybrid functionals. However, due to their computational

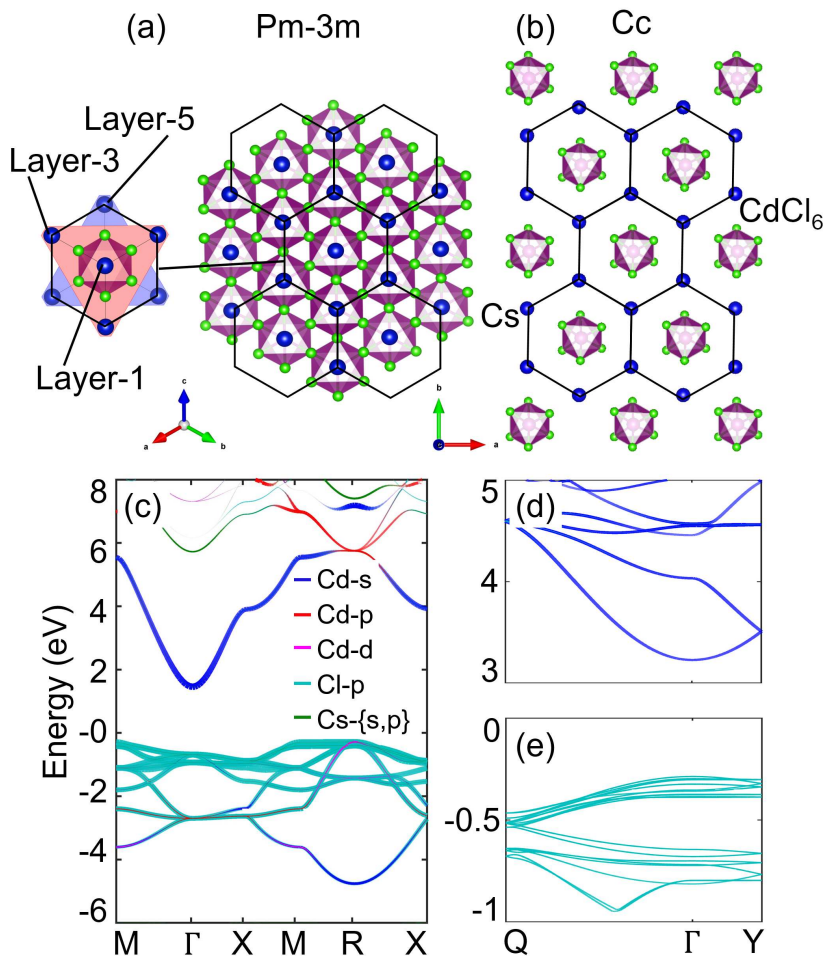


FIG. 1. Top view of the crystal structure of CsCdCl_3 in cubic phase projected along $[111]$ (a) and in a hypothetical monoclinic phase resembling that of the TMCM- CdCl_3 (b). The CdCl_6 octahedra complexes are shown. Orbital resolved band structure of cubic (c) and monoclinic (d-e) CsCdCl_3 .

cost they have not been applied for this study. Furthermore, in case of inorganic ferroelectric perovskites it was found that nonhybrid functionals outperform the hybrid ones for ferroelectricity-related properties [32].

Figure 2(c) shows the orbital resolved spin-orbit coupled band structure. The notable feature is spin splitting in the valence bands away from high symmetry k points (Q, Γ and Y). It should be noted that we find negligibly small spin splitting in the conduction band also. The Cc space group of TMCM- CdCl_3 is non-centrosymmetric and, therefore could exhibit spin polarizations (Rashba and/or Dresselhaus type) [10]. Figure 3 gives the two highest energy valence bands and their two dimensional cross sections. We find spin-splitting along k_x and k_y directions, but no splitting along k_z direction. To gain further understanding and quantify spin-splitting we develop an effective Hamiltonian for the structure. TMCM- CdCl_3 belongs to C_s point group symmetry, which has mirror plane M_y (see Fig. 2a). Table I lists symmetry invariants under all relevant symmetry operations as reported in Ref.14.

TABLE I. Symmetry operators and corresponding invariants for C_s point group symmetry.

Symmetry	(k_x, k_y, k_z)	$(\sigma_x, \sigma_y, \sigma_z)$	Invariants
$T = i\sigma_y K$	$(-k_x, -k_y, -k_z)$	$(-\sigma_x, -\sigma_y, -\sigma_z)$	$k_x\sigma_x, k_x\sigma_y, k_x\sigma_z$ $k_y\sigma_x, k_y\sigma_y, k_y\sigma_z$ $k_z\sigma_x, k_z\sigma_y, k_z\sigma_z$
$M_y = i\sigma_y$	$(k_x, -k_y, k_z)$	$(-\sigma_x, \sigma_y, -\sigma_z)$	$k_x\sigma_y, k_z\sigma_y$ $k_y\sigma_x, k_y\sigma_z$

The effective Hamiltonian is constructed by retaining common invariants from all the symmetry operations, and is

$$H = \frac{\hbar^2}{2} \left(\frac{k_x^2}{m_x} + \frac{k_y^2}{m_y} + \frac{k_z^2}{m_z} \right) + \alpha k_x \sigma_y + k_y (\beta \sigma_x + \gamma \sigma_z) + k_z \delta \sigma_y \quad (1)$$

where α, β, γ and δ are the adjustable parameters which can be obtained from fitting the eigenvalues of the Hamiltonian to the DFT computed ones. For example, for k_y -

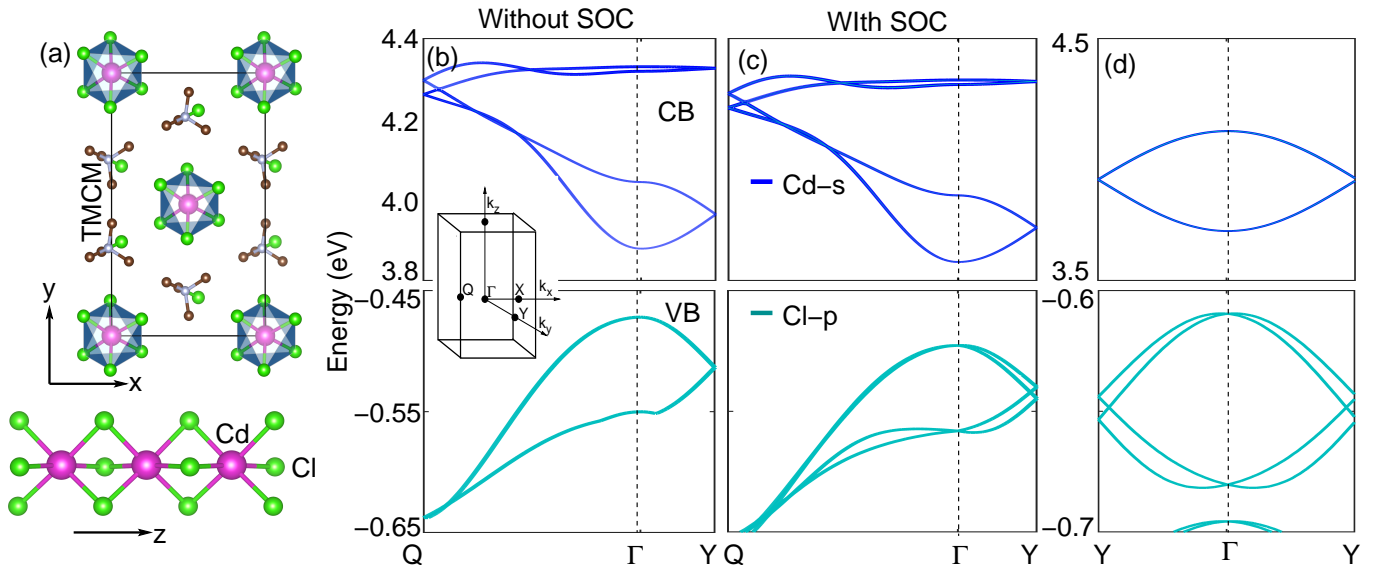


FIG. 2. (a) Conventional cell of TMCM-CdCl₃ and chain of CdCl₆ octahedra. TMCM molecules in the unit cell are presented without hydrogen atoms. Orbital resolved band structure of TMCM-CdCl₃ in absence (b) and presence (c) of SOC. Band structure along Y-Γ-Y path, where the spin splitting is maximum (d). The inset in (b) shows the Brillouin zone.

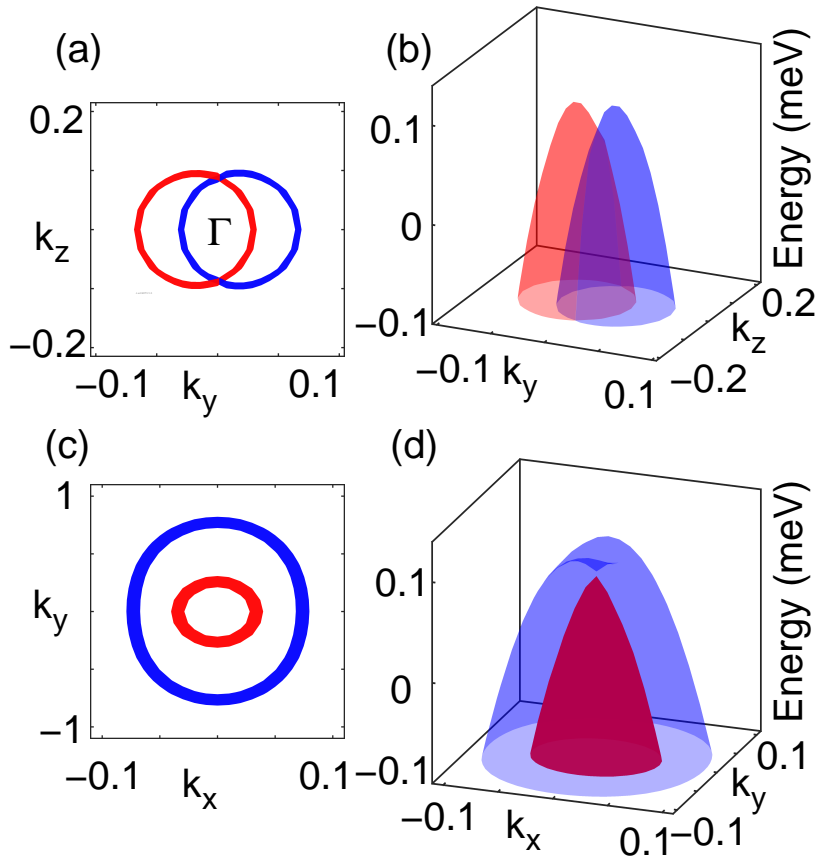


FIG. 3. Two dimensional cross section of valence bands for 5 meV ranges in different planes (a) and (c), and corresponding three dimensional plot (b) and (d). The two bands shown in red and blue corresponds to spin-up and spin-down channels; k_x , k_y and k_z are multiple of $2\pi/a$, $2\pi/b$ and $2\pi/c$, respectively and in units of \AA^{-1} .

k_z plane the matrix form of the Hamiltonian is

$$H = \begin{pmatrix} \frac{\hbar^2}{2} \left(\frac{k_y^2}{m_y} + \frac{k_z^2}{m_z} \right) + k_y \gamma & \beta k_y - i \delta k_z \\ \beta k_y + i \delta k_z & \frac{\hbar^2}{2} \left(\frac{k_y^2}{m_y} + \frac{k_z^2}{m_z} \right) - k_y \gamma \end{pmatrix} \quad (2)$$

Technically, we fit DFT band structure along directions Y- Γ -Y, X- Γ -X, and Z- Γ -Z separately. We numerically find eigenvalues of the Hamiltonian for the given direction and adjust the fitting parameters until good match with DFT predictions is achieved. Alternatively, we derived analytical expressions for the eigenvalues and eigenvectors of the Hamiltonian for different planes and used the former one to fit DFT band structure. Both technical approaches yielded the same values of the adjustable parameters.

TABLE II. Effective interaction (t_x , t_y , and t_z) and spin splitting strengths (α - δ) in $\text{meV}\text{\AA}^{-2}$ and $\text{meV}\text{\AA}$, respectively.

Compound	t_x	t_y	t_z	α	β	γ	δ
TMCM-CdCl ₃	-3.7	-4.8	-26.0	1.0	0.0	1.6	0.1
TMBM-CdBr ₃	-4.6	-10	-27.5	2.5	2.5	6	2.5
TMBM-CdCl ₃	-5.3	-7.5	-25	2	0	2.5	1
TMCM-CdBr ₃	-2.2	-6	-28	8	0	2.8	3
CsCdCl ₃	-5	0.1	-19	0.3	0	0.6	0.1

All the fitted parameters are listed in Table II, where we use $t_i = \frac{\hbar^2}{2m_i} [i = x, y, z]$ as the parameters that determine the curvature of the band. Analysis of the parameters strength indicates that effective masses are k -dependent and have larger value along k_x direction. In case of TMCM-CdCl₃ we find that among the parameters that control spin-splitting the largest values are for γ and α which explain the large splitting along k_y and k_x directions.

The expectation value of spinors, $\sigma_i (i = x, y, z)$, give rise to finite value of σ_z component which is proportional to spin splitting parameter γ . Other components σ_x and σ_y mainly depend on the β and δ , whose values are very small. Thus, the TMCM-CdCl₃ exhibits persistent spin texture given in Fig. 4a. In the case of k_x - k_y plane (Fig. 4b) the spin-texture as predicted by the effective Hamiltonian is of Dresselhaus type. However, due to negligible strength of β splitting parameter σ_x is nearly zero and spin texture appears to be persistent in nature.

V. CHEMICAL AND ELECTRICAL TUNABILITY OF SPIN POLARIZATIONS

Next we set to understand the role that TMCM molecule plays in the spin-splitting. For that we replace the molecule with Cs placed on the N site of TMCM. No structural relaxation is performed here as we are interested just in the contribution of the TMCM molecule. The calculated band structure of the CsCdCl₃ monoclinic conventional cell is shown in the Fig. 5(a). Interestingly,

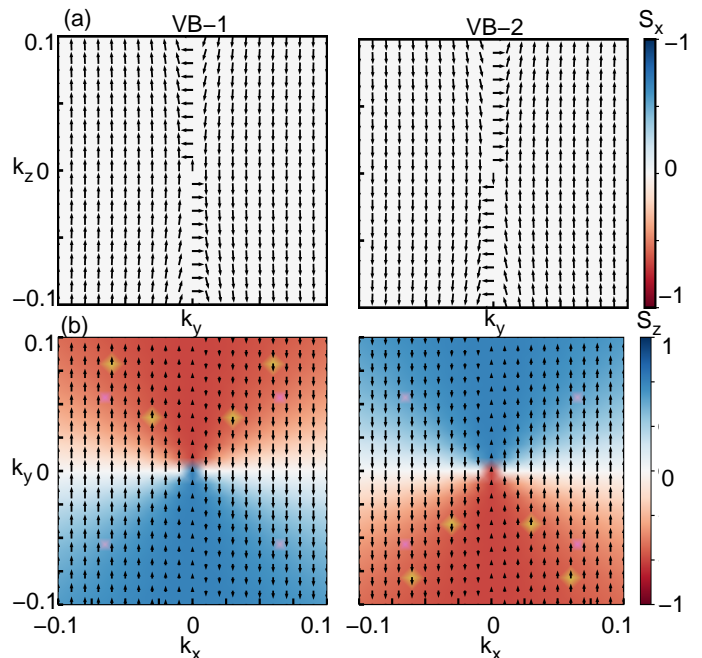


FIG. 4. Spin texture of valence bands of TMCM-CdCl₃ in k_y - k_z (a) and k_x - k_y (b) planes, obtained from effective model Hamiltonian.

the splitting in the valence band has reduced to negligibly small values, despite the fact that the supercell exhibits spontaneous polarization of $3.5 \mu\text{C}/\text{cm}^2$ that is comparable with TMCM-CdCl₃ one. The finding suggests that it is the spatial charge distribution of the organic molecule that is responsible for the spin splitting. Consequently, one may wonder whether the spin splitting is tunable by the organic molecule.

To answer this question we extend our investigation to fluorine substituted $\text{TMC}_{1-x}\text{F}_x\text{M-CdCl}_3$ (TMCFM) ($x = 0.25$), which crystallize in the same Cc space group [17]. Technically, we replaced one TMCM molecule with TMFM in the ground state structure of TMCM-CdCl₃ and carried out full structural relaxation. Both spin splitting and polarization indeed changed in this case, although rather slightly (see Fig. 5b). The values are reported in Table III. As the next substitution we replaced Cl by Br in the TMCM molecule and carried out full structural relaxation. In this case we find larger change in the polarization with respect to TMCM-CdCl₃ and nearly 50% increase in the spin splitting (see Fig. 5c and Table III), which indeed confirm tunability of the spin-splitting by the choice of the organic molecule and may open a way to property engineering.

To further explore tunability of spin-splitting in this family of compounds we recall that the conduction and valence band edges are dominated by B and X sites, respectively. We hypothesize that replacing Cl with Br on the X site will lead to enhancement of the spin-splitting due to larger atomic SOC of Br. To test the hypothesis we carried out band structure calculation for various

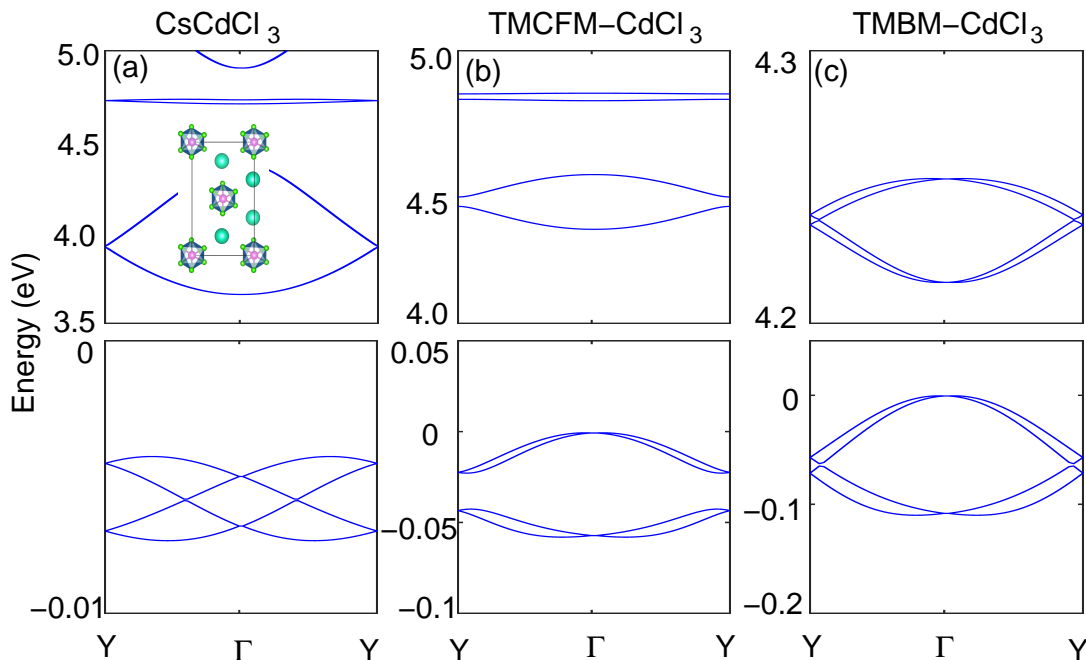


FIG. 5. Band structure of monoclinic CsCdCl_3 (a), $\text{TMC}_{1-x}\text{F}_x\text{M-CdCl}_3$ with $x=0.25$ (b), and TMBM-CdCl_3 (c). Note the difference in the energy scale.

TABLE III. Band-splitting computed at $(0, 0.025, 0)$ point of Brillouin zone and polarizations for various HOIPs.

Compound	Splitting Energy (meV)	Polarization ($\mu\text{C}/\text{cm}^2$)
TMCM-CdCl_3	0.11	$(-3.3, 0, 4.5)$
$\text{TMC}_{1-x}\text{F}_x\text{M-CdCl}_3$ ($x = 0.25$)	0.09	$(-3.5, 0.0, 4.4)$
TMBM-CdCl_3	0.15	$(-2.5, 0, 4.6)$
TMCM-CdBr_3	0.38	$(-2.8, 0, 4.3)$
TMBM-CdBr_3	0.91	$(-2.3, 0, 4.3)$
CsCdCl_3	0.00	$(3.9, 0, -4.4)$

combinations of Cl and Br atoms on organic molecule site and on X site of ABX_3 , without altering the symmetry of the cell. We considered TMBM-CdBr_3 and TMCM-CdBr_3 in Cc space group. Among these compounds, TMCM-CdBr_3 is experimentally synthesized in space group $P6_3mc$ [33]. The computed band structure is presented in the Fig. 6 and spin-splittings and polarizations are listed in Table III. The data reveal that for TMBM-CdBr_3 and TMCM-CdBr_3 the spin splitting is enhanced by nine times and three times, respectively, as compared to TMCM-CdCl_3 band splitting. In addition, we now observe small splitting in conduction bands of TMBM-CdBr_3 and TMBM-CdCl_3 . This is further illustrated in the strengths of the effective Hamiltonian coupling parameters in Table II. Br-based compounds have significantly larger values as compared to Cl, while CsCdCl_3 has the smallest splitting strength among all.

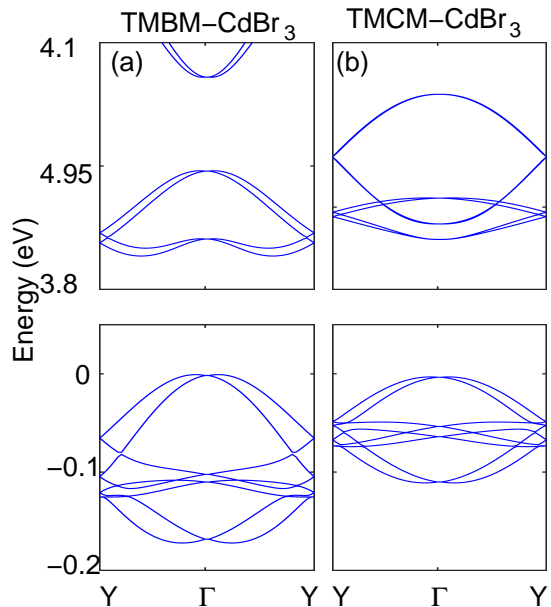


FIG. 6. Band structure of monoclinic TMBM-CdBr_3 (a) and TMCM-CdBr_3 (b).

We attribute these findings to the larger atomic number of Br compared to Cl which enhances atomic SOC.

One of the most attractive properties of the co-functionality is the possibility to control spin polarizations by reversal of ferroelectric polarization. To test this in TMCM-CdCl_3 , we inverted the ground state structure as suggested in Ref. 34 and repeated simulations. The

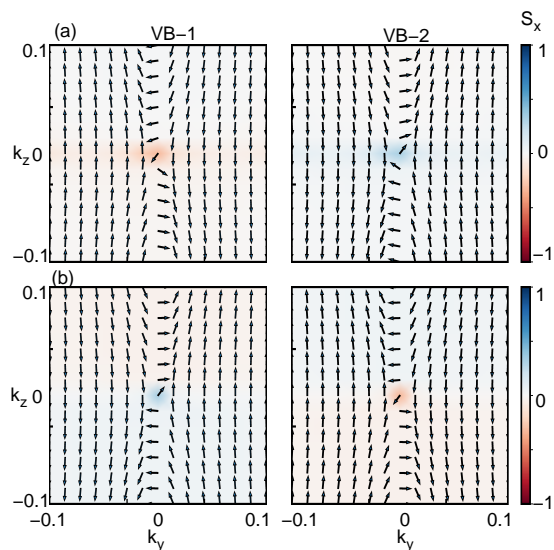


FIG. 7. Spin texture of valence bands of TCMC-CdCl₃ for 10 $\bar{1}$ polarization direction (a) and for $\bar{1}01$ polarization direction (b). The system exhibits the persistent spin texture oriented along k_z direction and the direction is reversed for opposite direction of polarization.

polarization reversed its direction which resulted in reversal of spin textures as shown in Fig. 7b. This finding confirms the tunability of spin texture in this material by the electric polarization.

VI. SUMMARY

In summary, we have used DFT-based computations to investigate electronic structure of Cd-based HOIP and the effect that SOC has on it. We found that in the

parent compound, cubic CsCdCl₃ conduction and valence band edges are dominated by Cd-s and Cl-p and originate from Cd-{s, p}-Cl-p molecular orbitals. This insight suggested the possibility to chemically tune the band edges through substitution on the X site. In the TCMC-CdCl₃ compound we found band splitting due to SOC. Such splitting is indeed allowed in this material as its structure lacks inversion symmetry. Interestingly, the spin-splitting was found to correlate not as much with the material's polarization as with the spacial charge distribution introduced by the organic molecule. An effective Hamiltonian is proposed to gain insights into band-splitting and spin polarization. Interestingly, it predicts the Dresselhaus type of spin splitting in the Cc space group which, however, results in persistent spin textures in the materials studied due to the delicate interplay of the interaction strengths. From the practical perspective the persistent spin textures are very attractive as they found to be fully controllable by the polarization direction, which, in turn, can be manipulated by the electric field. Another finding that is also of practical significance is the high chemical tunability of the spin-polarization. For example, replacing Cl with Br results in the ten times increase of the band splitting which we attribute to the higher atomic SOC of Br. Thus, the study reveals both scientific and technological appeal of these emerging materials.

VII. ACKNOWLEDGEMENT

This work is supported by the U.S. Department of Energy, Office of Basic Energy Sciences, Division of Materials Sciences and Engineering under grant DE-SC0005245. BRKN acknowledges the support from DST, India under grant CRG/2020/004330.

-
- [1] J. F. Scott, Applications of modern ferroelectrics, *Science* **315**, 954–959 (2007).
 - [2] Andrew M. Martin, Lane W. Rappe, Thin-film ferroelectric materials and their applications, *Nature Reviews Materials* **2** (2016)..
 - [3] J. Krempaský, S. Muff, J. Minár, N. Pilet, M. Fanciulli, A. P. Weber, E. B. Guedes, M. Caputo, E. Müller, V. V. Volobuev, M. Gmitra, C. A. F. Vaz, V. Scagnoli, G. Springholz, and J. H. Dil, Operando imaging of all-electric spin texture manipulation in ferroelectric and multiferroic Rashba semiconductors, *Phys. Rev. X* **8**, 021067 (2018).
 - [4] J. Krempaský, S. Muff, F. Bisti, M. Fanciulli, H. Volfová, A. P. Weber, N. Pilet, P. Warnicke, H. Ebert, J. Braun, F. Bertran, V. V. Volobuev, J. Minár, G. Springholz, J. H. Dil, and V. N. Strocov, Entanglement and manipulation of the magnetic and spin-orbit order in multiferroic Rashba semiconductors, *Nature Communications* **7** (2016)..
 - [5] Domenico Di Sante, Paolo Barone, Riccardo Bertacco, and Silvia Picozzi, Electric control of the giant Rashba effect in bulk GeTe, *Advanced Materials* **25**, 509–513 (2013).
 - [6] Christian Rinaldi, Sara Varotto, Silvia Asa, Picozzi, and Riccardo Bertacco, Ferroelectric control of the spin texture in GeTe, *Nano Letters* **18**, 2751–2758 (2018).
 - [7] Carlos Mera Acosta, Adalberto Fazzio, Gustavo M. Dalpian, and Alex Zunger, Inverse design of compounds that have simultaneously ferroelectric and Rashba co-functionality, *Physical Review B* **102**, 144106 (2020).
 - [8] Xiuwen Zhang, Qihang Liu, Jun Wei Luo, Arthur J. Freeman, and Alex Zunger, Hidden spin polarization in inversion-symmetric bulk crystals, *Nature Physics* **10**, 387–393 (2014).
 - [9] Lin Ding Yuan, Zhi Wang, Jun Wei Luo, Emmanuel I. Rashba, and Alex Zunger, Giant momentum-dependent spin splitting in centrosymmetric low-Z antiferromagnets, *Physical Review B* **102**, 14422 (2020).

- [10] Carlos Mera Acosta, Elton Ogoshi, Adalberto Fazzio, Gustavo M. Dalpian, and Alex Zunger, The rashba scale: Emergence of band anti-crossing as a design principle for materials with large rashba coefficient, *Matter* **3**, 145–165 (2020).
- [11] Hong Jian Zhao, Peng Chen, Charles Paillard, Rémi Arras, Yue-Wen Fang, Xu Li, Julien Gosteau, Yurong Yang, and Laurent Bellaiche, Large spin splittings due to the orbital degree of freedom and spin textures in a ferroelectric nitride perovskite, *Phys. Rev. B* **102**, 041203 (2020).
- [12] J. Gosteau, R. Arras, P. Chen, H. J. Zhao, C. Paillard, and L. Bellaiche, Spin-orbit effects in ferroelectric PbTiO_3 under tensile strain, *Phys. Rev. B* **103**, 024416 (2021).
- [13] Hong Jian Zhao, Hiro Nakamura, Rémi Arras, Charles Paillard, Peng Chen, Julien Gosteau, Xu Li, Yurong Yang, and Laurent Bellaiche, Purely cubic spin splittings with persistent spin textures, *Phys. Rev. Lett.* **125**, 216405 (2020).
- [14] L L Tao and Evgeny Y Tsymbal, Perspectives of spin-textured ferroelectrics, *Journal of Physics D: Applied Physics* **54**, 113001 (2021).
- [15] Yu Meng You, Wei Qiang Liao, Dewei Zhao, Heng Yun Ye, Yi Zhang, Qionghua Zhou, Xianghong Niu, Jinlan Wang, Peng Fei Li, Da Wei Fu, Zheming Yang, Song Gao, Kunlun Yang, Jun Ming Liu, Jiangyu Li, Yanfa Yan, and Ren Gen Xiong, An organic-inorganic perovskite ferroelectric with large piezoelectric response, *Science* **357**, 306–309 (2017).
- [16] Wei Qiang Liao, Yuan Yuan Tang, Peng Fei Li, Yu Meng You, and Ren Gen Xiong, Large Piezoelectric Effect in a Lead-Free Molecular Ferroelectric Thin Film, *Journal of the American Chemical Society* **139**, 18071–18077 (2017).
- [17] Wei Qiang Liao, Dewei Zhao, Yuan Yuan Tang, Yi Zhang, Peng Fei Li, Ping Ping Shi, Xiao Gang Chen, Yu Meng You, and Ren Gen Xiong, A molecular perovskite solid solution with piezoelectricity stronger than lead zirconate titanate, *Science* **363**, 1206–1210 (2019).
- [18] Daibei Yang, Lingheng Luo, Yi Gao, Shuang Chen, and Xiao Cheng Zeng, Rational design of one-dimensional hybrid organic-inorganic perovskites with room-temperature ferroelectricity and strong piezoelectricity, *Materials Horizons* **6**, 1463–1473 (2019).
- [19] Minsung Kim, Jino Im, Arthur J. Freeman, Jisoon Ihm, and Hosub Jin, Switchable $s = 1/2$ and $j = 1/2$ rashba bands in ferroelectric halide perovskites, *Proceedings of the National Academy of Sciences* **111**, 6900–6904 (2014).
- [20] Feng Lou, Teng Gu, Junyi Ji, Junsheng Feng, Hongjun Xiang, and Alessandro Stroppa, Tunable spin textures in polar antiferromagnetic hybrid organic-inorganic perovskites by electric and magnetic fields, *npj Computational Materials* **6**, 1–9 (2020).
- [21] P. S. Ghosh, Sergey Lisenkov, and Inna Ponomareva, Phase switching as the origin of large piezoelectric response in organic-inorganic perovskites: A first-principles study, *Phys. Rev. Lett.* **125**, 207601 (2020).
- [22] P. S. Ghosh, J. Doherty, S. Lisenkov, and I. Ponomareva, Tunability of structure, polarization, and band gap of high tc organic-inorganic ferroelectrics by hydrostatic pressure: First-principles study, *The Journal of Physical Chemistry C* **125**, 16296–16303 (2021).
- [23] J. P. Perdew, K. Burke, and M. Ernzerhof, *Phys. Rev. Lett.* **77**, 3865–3868 (1996).
- [24] G. Kresse and J. Furthmüller, Efficient iterative schemes for ab initio total-energy calculations using a plane-wave basis set, *Phys. Rev. B* **54**, 11169–11186 (1996).
- [25] P. E. Blöchl, *Phys. Rev. B: Condens. Matter Mater. Phys.* **50**, 17953 (1994).
- [26] S. Grimme, Semiempirical GGA-type Density Functional Constructed with a Long range Dispersion Correction, *J. Comput. Chem.* **27**, 1787 (2006).
- [27] R. D. King-Smith and David Vanderbilt, Theory of polarization of crystalline solids, *Phys. Rev. B* **47**, 1651–1654 (1993).
- [28] Roberto L. Moreira and Anderson Dias, Comment on prediction of lattice constant in cubic perovskites, *Journal of Physics and Chemistry of Solids* **68**, 1617–1622 (2007).
- [29] L.Q. Jiang, J.K. Guo, H.B. Liu, M. Zhu, X. Zhou, P. Wu, and C.H. Li, Prediction of lattice constant in cubic perovskites, *Journal of Physics and Chemistry of Solids* **67**, 1531–1536 (2006).
- [30] Ravi Kashikar, Mayank Gupta, and B. R. K. Nanda, A generic slater-koster description of the electronic structure of centrosymmetric halide perovskites, *The Journal of Chemical Physics* **154**, 104706 (2021).
- [31] Centimeter-sized molecular perovskite crystal for efficient x-ray detection, *Advanced Functional Materials* **31**, 2100691 (2021).
- [32] Maggie Kingsland, K. A. Lynch, S. Lisenkov, Xiao He, and I. Ponomareva, Comparative study of minnesota functionals performance on ferroelectric BaTiO_3 and PbTiO_3 , *Phys. Rev. Materials* **4**, 073802 (2020).
- [33] Wei-Qiang Liao, Yuan-Yuan Tang, Peng-Fei Li, Yu-Meng You, and Ren-Gen Xiong, Competitive halogen bond in the molecular ferroelectric with large piezoelectric response, *Journal of the American Chemical Society* **140**, 3975–3980 (2018).